Efficient Image Dehazing with Boundary Constraint and Contextual Regularization

Gaofeng MENG, Ying WANG, Jiangyong DUAN, Shiming XIANG, Chunhong PAN

National Laboratory of Pattern Recognition
Institute of Automation, Chinese Academy of Science, Beijing, P.R. China
Email:{gfmeng,ywang,jyduan,smxiang,chpan}@nlpr.ia.ac.cn

***Abstract*—Images captured in foggy weather conditions often suffer from bad visibility. In this paper, we propose an efficient regularization method to remove hazes from a single input image. Our method benefits much from an exploration on the inherent boundary constraint on the transmission function. This constraint, combined with a weighted L_1-norm based contextual regularization, is modeled into an optimization problem to estimate the unknown scene transmission. A quite efficient algorithm based on variable splitting is also presented to solve the problem. The proposed method requires only a few general assumptions and can restore a high-quality haze-free image with faithful colors and fine image details. Experimental results on a variety of haze images demonstrate the effectiveness and efficiency of the proposed method.**

***Keywords*-image processing; single image dehazing; visibility enhancement;**

I. Introduction

When one takes a picture in foggy weather conditions, the obtained image often suffers from poor visibility. The distant objects in the fog lose the contrasts and get blurred with their surroundings, as illustrated in Figure 1. This is because the reflected light from these objects, before it reaches the camera, is attenuated in the air and further blended with the atmospheric light scattered by some aerosols (*e.g.*, dust and water-droplets). Also for this reason, the colors of these objects get faded and become much similar to the fog, the similarity of which depending on the distances of them to the camera.

Early methods for haze removal mainly rely on additional depth information or multiple observations of the same scene. Representative works include [11], [9], [10], [12]. Schechner *et al.* [11] notice that the airlight scattered by atmospheric particles is partially polarized. Based on this observation, they develop a quick method to reduce hazes by using two images taken through a polarizer at different angles. Narasimhan *et al.* propose a physics-based scattering model [9], [10]. By this model, the scene structure can be recovered from two or more weather images. Kopf *et al.* [6] propose to dehaze an image by using the scene depth information directly accessible in the georeferenced digital terrain or city models.

Figure 1. Image dehazing result by our method. From left to right: (Top) the foggy image and the dehazing result by our method. (Bottom) the boundary constraint map and the recovered scene transmission.

Single image dehazing, in contrast, is a more challenging problem, since fewer information about the scene structure is available. Recently, some significant advances have also been achieved [4], [13], [5], [14], [7], [8]. These progresses benefit much from the insightful explorations on new image models and priors. Fattal [4] proposes a refined image formation model to account for the surface shading and the scene transmission. Under the assumption that the two functions are locally statistically uncorrelated, a haze image can be broken into regions of constant albedo, from which the scene transmission can be inferred. Tan [13] proposes to enhance the visibility of a haze image by maximizing its local contrast. His method can generate quite compelling results, especially in regions with very dense hazes. However, since it is not a physics-based method, the restored image often suffers from distorted colors and significant halos.

He *et al.* [5] present an interesting image prior - *dark channel prior* for single image dehazing. This prior comes from an observation that most local patches in haze-free images often contain some low intensity pixels. The prior,

combined with a soft-mating operation, can achieve a quite compelling haze-free result of very high quality. Kratz *et al.* [7] model an image as a factorial Markov random field, in which the scene albedo and depth are two statistically independent latent layers. A canonical expectation maximization algorithm is implemented to factorize the image. Kratz's method can recover a haze-free image with fine edge details, but the results often tend to be over enhanced.

Single image dehazing is essentially an under-constrained problem. The general principle of solving such problems is therefore to explore additional priors or constraints. Following this idea, we begin our study in this paper by deriving an inherent boundary constraint on the scene transmission. This constraint, combined with a weighted L_1-norm based contextual regularization between neighboring pixels, is formalized into an optimization problem to recover the unknown transmission. Our method requires only a few general assumptions and can restore a haze-free image of high quality with faithful colors and fine edge details. Figure 1 illustrates an example of our dehazing result.

Our method benefits from three main contributions. The first is a new constraint on the scene transmission. This simple constraint, which has a clear geometric interpretation, shows to be surprisingly effective to image dehazing. Our second contribution is a new contextual regularization that enables us to incorporate a filter bank into image dehazing. These filters help in attenuating the image noises and enhancing some interesting image structures, such as jump edges and corners. Our final contribution is an efficient optimization scheme, which enable us to quickly dehaze images of large sizes.

II. Imaging Model and Problem Constraints

The following linear interpolation model is widely used to explain the formation of a haze image [10], [4], [5], [13], [7]:

$$\mathbf{I}(x) = t(x)\mathbf{J}(x) + (1 - t(x))\mathbf{A}, \tag{1}$$

where $\mathbf{I}(x)$ is the observed image, $\mathbf{J}(x)$ is the scene radiance, $\mathbf{A}$ is the global atmospheric light, and $t(x)$ is the scene transmission. The transmission function $t(x)$ $(0 \leq t(x) \leq 1)$ is correlated with the scene depth. Further assuming that the haze is homogenous, we can express $t(x)$ as follows:

$$t(x) = e^{-\beta d(x)}, \tag{2}$$

where β is the medium extinction coefficient, and $d(x)$ is the scene depth.

The goal of image dehazing is to recover the scene radiance $\mathbf{J}(x)$ from $\mathbf{I}(x)$ based on Eq.(1). This requires us to estimate the transmission function $t(x)$ and the global atmospheric light $\mathbf{A}$. Once $t(x)$ and $\mathbf{A}$ are estimated, the scene radiance can be recovered by:

$$\mathbf{J}(x) = \frac{\mathbf{I}(x) - \mathbf{A}}{[\max(t(x), \epsilon)]^{\delta}} + \mathbf{A}, \tag{3}$$

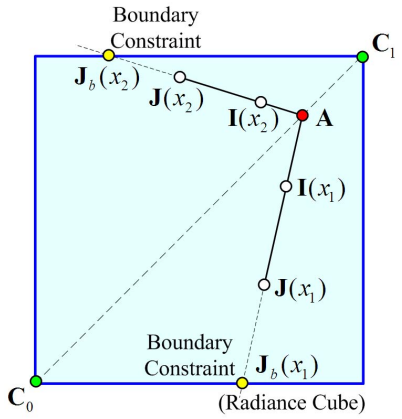

Figure 2. Radiance cube and boundary constraint. For each x, we require the extrapolation of $\mathbf{J}(x)$ cannot cross over the boundary of the radiance cube. $\mathbf{J}_b(x_1)$ and $\mathbf{J}_b(x_2)$ are the corresponding boundary constraint points.

where ϵ is a small constant (typically 0.0001) for avoiding division by zero, and the exponent δ, serving as the role of the medium extinction coefficient β in Eq.(2), is used for fine-tuning the dehazing effects.

However, dehazing from a single image is highly under-constrained, since the number of unknowns is much greater than the number of available equations. Thus, we have to first exploit more constraints on the unknowns.

A. Boundary Constraint from Radiance Cube

Geometrically, according to Eq.(1), a pixel $\mathbf{I}(x)$ contaminated by fog will be "*pushed*" towards the global atmospheric light $\mathbf{A}$ (see Figure 2). As a result, we can reverse this process and recover the clean pixel $\mathbf{J}(x)$ by a linear extrapolation from $\mathbf{A}$ to $\mathbf{I}(x)$. The appropriate amount of extrapolation is given by

$$\frac{1}{t(x)} = \frac{||\mathbf{J}(x) - \mathbf{A}||}{||\mathbf{I}(x) - \mathbf{A}||}. \tag{4}$$

Consider that the scene radiance of a given image is always bounded, that is,

$$\mathbf{C}_0 \leq \mathbf{J}(x) \leq \mathbf{C}_1, \forall x \in \Omega, \tag{5}$$

where $\mathbf{C}_0$ and $\mathbf{C}_1$ are two constant vectors that are relevant to the given image. Consequently, for any x, a natural requirement is that the extrapolation of $\mathbf{J}(x)$ must be located in the radiance cube bounded by $\mathbf{C}_0$ and $\mathbf{C}_1$, as illustrated in Figure 2.

The above requirement on $\mathbf{J}(x)$, in turn, imposes a boundary constraint on $t(x)$. Suppose that the global atmospheric light $\mathbf{A}$ is given. Thus, for each x, we can compute the corresponding boundary constraint point $\mathbf{J}_b(x)$ (see Figure 2). Then, a lower bound of $t(x)$ can be determined by using Eq.(4) and Eq.(5), leading to the following boundary constraint on $t(x)$:

$$0 \leq t_b(x) \leq t(x) \leq 1, \tag{6}$$

where $t_b(x)$ is the lower bound of $t(x)$, given by

$$t_b(x) = \min\left\{\max_{c\in\{r,g,b\}}\left(\frac{A^c - I^c(x)}{A^c - C_0^c}, \frac{A^c - I^c(x)}{A^c - C_1^c}\right), 1\right\}, \tag{7}$$

where I^c, A^c, C_0^c and C_1^c are the color channels of $\mathbf{I}$, $\mathbf{A}$, $\mathbf{C}_0$ and $\mathbf{C}_1$, respectively.

The boundary constraint of $t(x)$ provides a new geometric perspective to the famous dark channel prior [5]. Let $\mathbf{C}_0 = 0$ and suppose the global atmospheric light $\mathbf{A}$ is brighter than any pixel in the haze image. One can directly compute $t_b(x)$ from Eq.(1) by assuming the pixel-wise dark channel of $\mathbf{J}(x)$ to be zero. Similarly, assuming that the transmission in a local image patch is constant, one can quickly derive the patch-wise transmission $\tilde{t}(x)$ in He *et al.*'s method [5] by applying a maximum filtering on $t_b(x)$, i.e.,

$$\tilde{t}(x) = \max_{y\in\omega_x} t_b(y), \tag{8}$$

where ω_x is a local patch centered at x.

It is worth noting that the boundary constraint is more fundamental. In most cases, the optimal global atmospheric light is a little darker than the brightest pixels in the image. Those brighter pixels often come from some light sources in the scene, e.g., the bright sky or the headlights of cars. In these cases, the dark channel prior will fail to those pixels, while the proposed boundary constraint still holds.

It is also worthy to point out the commonly used constant assumption on the transmission within a local image patch is somewhat demanding. For this reason, the patch-wise transmission $\tilde{t}(x)$ based on this assumption in [5] is often underestimated. Here, we present a more accurate patch-wise transmission, which relaxes the above assumption and allows the transmissions in a local patch to be slightly different. The new patch-wise transmission is given as below:

$$\hat{t}(x) = \min_{y\in\omega_x}\max_{z\in\omega_y} t_b(z). \tag{9}$$

Fortunately, the above patch-wise transmission $\hat{t}(x)$ can be conveniently computed by directly applying a morphological closing on $t_b(x)$. Figure 3 illustrates a comparison of the dehazing results by directly using the patch-wise transmissions derived from dark channel prior and the boundary constraint map, respectively. One can observe that the patch-wise transmission from dark channel prior works not well in the bright sky region. The dehazing result also contains some halo artifacts. In comparison, the new patch-wise transmission derived from the boundary constraint map can handle the bright sky region very well and also produces fewer halo artifacts.

B. Weighted L_1-norm based Contextual Regularization

Generally, pixels in a local image patch will share a similar depth value. Based on this assumption, we have derived a patch-wise transmission from the boundary constraint. However, this contextual assumption often fails to image patches with abrupt depth jumps, leading to significant halo artifacts in the dehazing results.

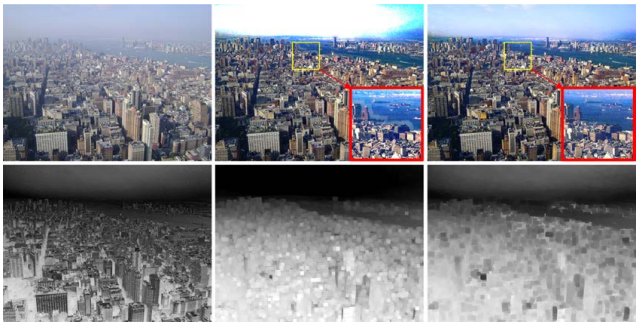

Figure 3. Image dehazing by directly using the patch-wise transmissions from dark channel prior and boundary constraint map, respectively. From left to right: (top) the foggy image, the dehazing result by dark channel prior and the dehazing result by boundary constraint. (bottom) the boundary constraint map, the patch-wise transmission from dark channel and the patch-wise transmission from boundary constraint map ($\mathbf{C}_0 = (20, 20, 20)^T$, $\mathbf{C}_1 = (300, 300, 300)^T$, $\delta = 1.0$, patch size: 17×17).

A trick to address this problem is to introduce a weighting function $W(x, y)$ on the constraints, i.e.,

$$W(x, y)\,(t(y) - t(x)) \approx 0, \tag{10}$$

where x and y are two neighboring pixels. The weighting function plays a "*switch*" role of the constraint between x and y. When $W(x, y) = 0$, the corresponding contextual constraint of $t(x)$ between x and y will be canceled.

The question now is how to choose a reasonable $W(x, y)$. Obviously, the optimal $W(x, y)$ is closely related to the depth difference between x and y. In another word, $W(x, y)$ must be small if the depth difference between x and y is large, and vice versa. However, since no depth information of each pixel is available in single image dehazing, we cannot construct $W(x, y)$ directly from the depth map.

Notice the facts that the depth jumps generally appear at the image edges, and that within local patches, pixels with a similar color often share a similar depth value. Consequently, we can compute the color difference of local pixels to construct the weighting function. Here below are two examples of the construction of such weighting functions. One is based on the squared difference between the color vectors of two neighboring pixels:

$$W(x, y) = e^{-\|\mathbf{I}(x)-\mathbf{I}(y)\|^2/2\sigma^2}, \tag{11}$$

where σ is a prescribed parameter. The other is based on the luminance difference of neighboring pixels [3], given as below:

$$W(x, y) = \left(|\ell(x) - \ell(y)|^\alpha + \epsilon\right)^{-1}, \tag{12}$$

where ℓ is the log-luminance channel of the image $\mathbf{I}(x)$, the exponent $\alpha > 0$ controls the sensitivity to the luminance difference of two pixels and ϵ is a small constant (typically 0.0001) for preventing division by zero.

Integrating the weighted contextual constraints in the whole image domain leads to the following contextual regularization on $t(x)$:

$$\int_{x\in\Omega}\int_{y\in\omega_x} W(x,y)\,|t(x)-t(y)|\,dxdy, \tag{13}$$

where Ω is the image domain. Instead of using the integral of L_2-norm for the regularization, we employ the integral of L_1-norm. This is because that L_1-norm is generally more robust to outliers than L_2-norm. These outliers appear when erroneous contextual constraints are introduced. For example, if two neighboring pixels with a similar color have very different depth values, Eq.(10) will provide an erroneous constraint.

To facilitate the computation, we further give the discrete form of (13) as below:

$$\sum_{i\in I}\sum_{j\in\omega_i} w_{ij}\,|t_i-t_j|, \tag{14}$$

where I is the index set of image pixels, w_{ij} is the discrete versions of $W(x,y)$. Exchanging the summation order in (14) and introducing a set of differential operators, we can further rewrite (14) as:

$$\sum_{j\in\omega}\sum_{i\in I} w_{ij}\,\left|(D_j\otimes t)_i\right|, \tag{15}$$

or more compactly,

$$\sum_{j\in\omega}\left\|W_j\circ(D_j\otimes t)\right\|_1, \tag{16}$$

where ω is an index set, $\circ$ represents the element-wise multiplication operator, $\otimes$ stands for the convolution operator, D_j is a first-order differential operator, W_j $(j\in\omega)$ is a weighting matrix.

It is also beneficial to use the high-order differential operators in (19). This simple extension endows us with more flexibilities in the use of the contextual constraints. Figure 4 shows a bank of high-order differential filters used in this study. To employ those filters, we have to accordingly revise the computation of the weighting functions in (11) and (12) as below:

$$W_j(i)=e^{-\sum_{c\in\{r,g,b\}}\left|(D_j\otimes I^c)_i\right|^2/2\sigma^2}, \tag{17}$$

$$W_j(i)=\left(\left|(D_j\otimes\ell)_i\right|^\alpha+\epsilon\right)^{-1}. \tag{18}$$

III. Scene Transmission Estimation

Dehazing an image by Eq.(3) requires to estimate an appropriate transmission function $t(x)$ and the global atmospheric light $\mathbf{A}$. To estimate the atmospheric light, He *et al.* [5] propose a method based on image's dark channel. They first pick up the top 0.1% brightest pixels in the dark channel, and then select the one with the highest intensity as the estimate of $\mathbf{A}$. In this study, we propose a modified

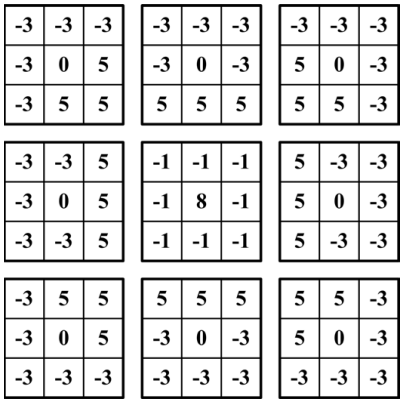

Figure 4. A bank of high-order filters used in our study. It consists of eight Kirsch operators and a Laplacian operator for preserving image edges and corners.

version of He *et al.*'s method. This method produces a similar result but performs more efficiently. The method begins with filtering each color channel of an input image by a minimum filter with a moving window. Then the maximum value of each color channel is taken as the estimate of the component of $\mathbf{A}$.

We find an optimal transmission function $t(x)$ by minimizing the following objective function:

$$\frac{\lambda}{2}\left\|t-\hat{t}\right\|_2^2+\sum_{j\in\omega}\left\|W_j\circ(D_j\otimes t)\right\|_1, \tag{19}$$

where the first part is the data term, which measures the fidelity of $t(x)$ to the patch-wise transmission $\hat{t}(x)$ derived from the boundary constraint map, the second part models the contextual constraints of $t(x)$, and λ is the regularization parameter for balancing the two terms.

To optimize (19), an efficient method based on variable splitting is employed. The basic idea of this method is to introduce several auxiliary variables and construct a sequence of simple sub-problems, the solutions of which finally converge to the optimal solution of the original problem. More specifically, we introduce the following auxiliary variables, denoted by u_j $(j\in\omega)$ and convert (19) to a new cost function as below:

$$\frac{\lambda}{2}\left\|t-\hat{t}\right\|_2^2+\sum_{j\in\omega}\left\|W_j\circ u_j\right\|_1+\frac{\beta}{2}\left(\sum_{j\in\omega}\left\|u_j-D_j\otimes t\right\|_2^2\right), \tag{20}$$

where β is a weight. Obviously, as $\beta\to\infty$, the solution of (20) will converge to that of (19).

Minimizing (20) for a fixed β can be performed by an alternating optimization with respect to u_j and t. That is, we first solve for each optimal u_j by fixing t, and then solve for an optimal t by fixing u_j. This process is repeated until convergence. Fortunately, the sub-problems of this process have close-form solutions that can be solved quite efficiently.

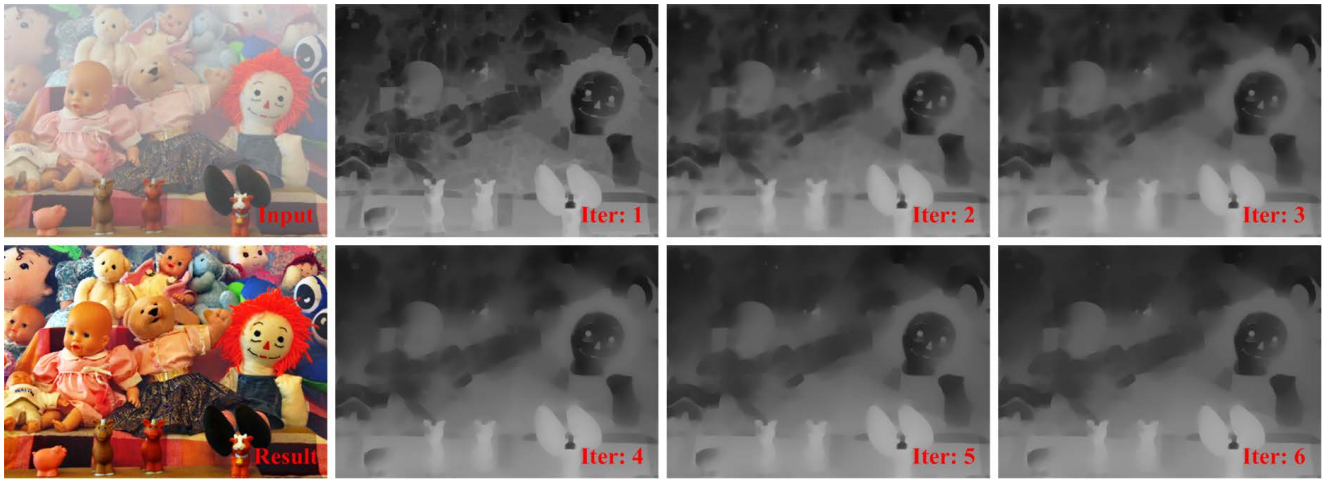

Figure 5. An example of scene transmission estimation. The estimation process quickly converges after a few iterations ($\mathbf{C}_0 = (20, 20, 20)^T, \mathbf{C}_1 = (300, 300, 300)^T$, $\lambda = 1.0$, $\alpha = 0.5$, patch size: 7×7).

Optimizing u_j: With t fixed in (20), we solve for u_j ($j \in \omega$) by minimizing the following function:

$$\|W_j \circ u_j\|_1 + \frac{\beta}{2} \|u_j - D_j \otimes t\|_2^2, \tag{21}$$

The above problem consists of solving a series of independent 1D problems of the following forms, i.e.,

$$\min_x |w \cdot x| + \tfrac{\beta}{2} (x - a)^2, \tag{22}$$

where w, β, and a are given. These problems can be directly solved as

$$x^* = \max\left(|a| - \frac{w}{\beta}, 0\right) \cdot sign(a), \tag{23}$$

where $sign(\cdot)$ is a sign function.

Optimizing t: We now find the optimal t by fixing $u_j (j \in \omega)$ in (20). This corresponds to minimizing the function below:

$$\frac{\lambda}{2} \left\|t - \hat{t}\right\|_2^2 + \frac{\beta}{2} \left(\sum_{j \in \omega} \|u_j - D_j \otimes t\|_2^2\right). \tag{24}$$

Note that (24) is quadratic in t. The optimal t thus satisfies:

$$\frac{\lambda}{\beta} \left(t - \hat{t}\right) + \sum_{j \in \omega} D_j^T \otimes (D_j \otimes t - u_j) = 0, \tag{25}$$

where D_j^T denotes the filter obtained by mirroring D_j around its center pixel. Applying a 2D FFT to the above equation and assuming the circular boundary conditions, we can compute the optimal t^* directly as:

$$t^* = \mathcal{F}^{-1}\left(\frac{\frac{\lambda}{\beta}\mathcal{F}\left(\hat{t}\right) + \sum_{j \in \omega} \overline{\mathcal{F}\left(D_j\right)} \circ \mathcal{F}\left(u_j\right)}{\frac{\lambda}{\beta} + \sum_{j \in \omega} \overline{\mathcal{F}\left(D_j\right)} \circ \mathcal{F}\left(D_j\right)}\right), \tag{26}$$

where $\mathcal{F}(\cdot)$ is the Fourier transform and $\mathcal{F}^{-1}(\cdot)$ is its inverse transform, $\overline{(\cdot)}$ represents the complex conjugate, and $\circ$ denotes the element-wise multiplication. The division in (26) is also performed in an element-wise manner.

Figure 5 illustrates an example of the estimation process of scene transmission function. In the process, we iteratively increase β from $\beta_0 = 1$ to $\beta_{Max} = 2^8$ by a scaling factor $2\sqrt{2}$, and alternatively solve the sub-problems in (21) and (24). For each round, we run only one inner iteration to optimize $t(x)$. The intermediate estimations of $t(x)$ and the final dehazing result are shown in the figure. We can see that the process quickly converges after a few iterations.

IV. Experimental Results

A. Example Results

Figure 6 illustrates some examples of our dehazing results and the recovered scene transmission functions. In the examples, we adopted the weighting functions in Eq.(18) and set the parameter $\alpha = 0.5$. The bank of high-order filters in Figure 4 are used to construct those weighting functions. The boundary constraint map is computed from Eq.(7) by setting the radiance bounds $\mathbf{C}_0 = (20, 20, 20)^T$ and $\mathbf{C}_1 = (300, 300, 300)^T$. We estimate the optimal transmission by minimizing the objective function in (19) and set the regularization parameter $\lambda = 1.0$ for all the examples.

As can be seen from the results, our method can recover rich details of images with vivid color information in the haze regions. It should be pointed out that the estimated transmissions of the right three images in the figure cannot be regarded as a scaling version of the depth map, since the hazes in the images are not homogeneous. These cases commonly occur to the captured scenes with a large area of clear sky region. Actually, the transmission function reflects the density of the hazes in the captured scene. From the

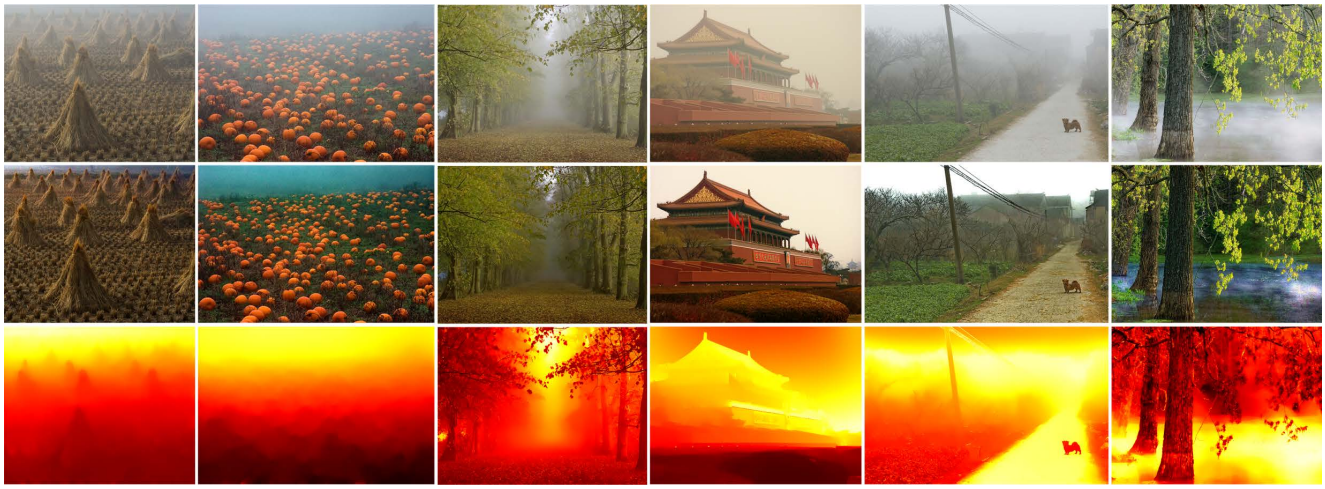

Figure 6. Image dehazing results by our method. Top: input haze images. Middle: the dehazing results. Bottom: the recovered transmission functions. The recovered transmission gives an estimation of the density map of hazes in the input image. (Best viewed in color)

figure, we can see the estimated transmissions by our method are quite consistent with our intuitions.

B. Comparisons

We also compare our method with several state-of-the-art methods. Figure 7 illustrates the comparisons of our method with Tan's work [13]. Tan's method can augment the image details and greatly enhance the image visuality. However, the colors in the recovered images are often over saturated, since the method is not a physically based approach and the transmission may thus be underestimated. Moreover, some significant halo artifacts usually appear around the recovered sharp edges (*e.g.*, trees). In comparison, our method can improve the visuality of image structures in very dense haze regions while restoring the faithful colors. The halo artifacts in our results are also quite small.

Figure 8 shows the comparisons of our approach with Tarel *et al.*'s method [14], [15] and Fattal's method [4]. Tarel *et al.*'s method is a filtering based approach. They estimate the atmospheric veil by applying a fast median filter to the minimum components of the observed image. The biggest advantage of their method is its linear complexity and can be implemented in real time, while the weakness is the dehazing results are not quite visually compelling. Fattal's method relies on sufficient color information to estimate the transmission. If the haze is very dense, the color information will be very faint and the transmission may thus be wrongly estimated, leading to erroneous enhancement on the image. For example, the hill enhanced by Fattal's method in Figure 8 is too dark (bottom image) and some hazes still remain among the underbrush (top image). In comparison, our results are much visually pleasing.

In Figure 9, we compare our approach with Kratz *et al.*'s method [7] and Ancuti *et al.*'s method [1]. Kratz *et al.*'s method adopts a factorial Markov random field to model a foggy image. By exploiting the priors of natural images and depth statistics, they can factorize the image into its scene albedo and depth via an EM algorithm. However, the method often tends to produce an over saturated result. Moreover, the dehazing results also contain some halo artifacts. Ancuti *et al.*'s method is a detection based method. It first computes the "*semi-inverse*" image by applying a pixel-wise operation on the input image. Based on the hue disparity between the original image and its semi-inverse, they can quickly identify the hazy regions and estimate the global airlight constant and the transmission map. Ancuti *et al.*'s method is quite efficient and can produce a visually pleasing result. However, due to the ambiguity between color and depth, pixel-wise haze detection is not robust and often suffers from large recognition errors. Therefore, some hazes in the images are not fully removed (*e.g.*, hazes among the trees). In contrast, our method can well remove most hazes in the image and produce a clear image with vivid color information.

We also compare our method with He *et al.*'s work in Figure 10. As can be seen from the results, the both methods produce comparable results in regions with heavy hazes (*e.g.*, the distant buildings). In regions with many depth jumps (*e.g.*, trees at close range), our method performs better. Fewer hazes remain in the our dehazing results and the halo artifacts are also smaller. Moreover, our method tends to generate a clearer result of image details, as illustrated in the second row of Figure 10. This benefits from the incorporation of a filter bank into image dehazing. These filters can help to exploit and augment the interesting image structures, e.g., jump edges and corners.

V. Discussion and Conclusion

In this paper, we have proposed an efficient method to remove hazes from a single image. Our method benefits

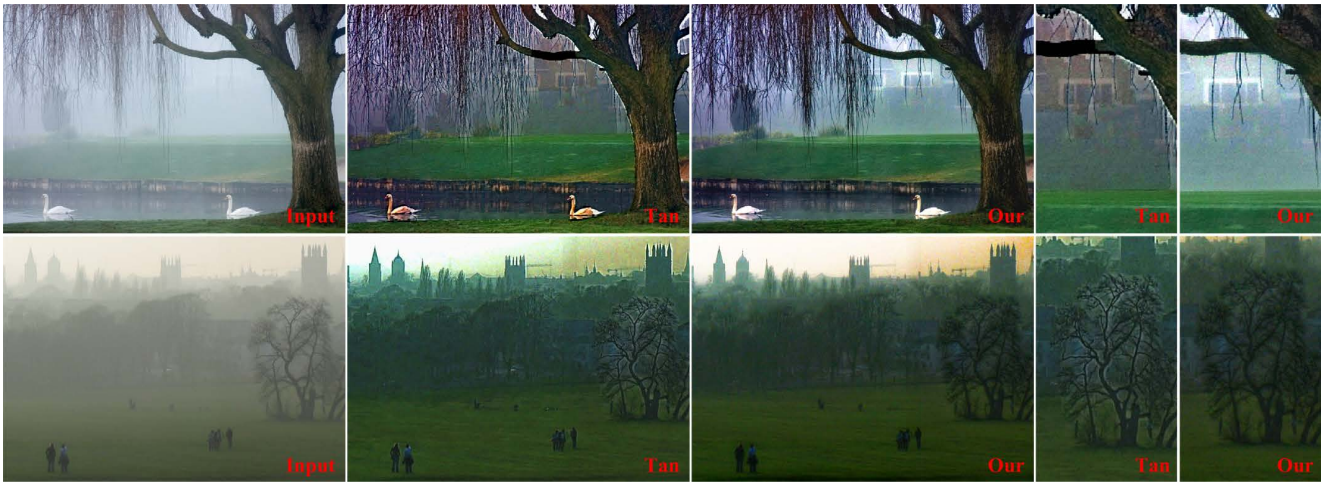

Figure 7. Comparisons with Tan's method. From left to right: input haze images, Tan's results, our results and the close-up patches of the results, respectively. (Best viewed in color)

Figure 8. Comparisons with Tarel *et al.*'s method and Fattal's method. From left to right: input haze images, the results of Tarel *et al.*'s method in ICCV'09, the results of Tarel *et al.*'s method in IV'10, Fattal's results, and our results, respectively. (Best viewed in color)

Figure 9. Comparison with Kratz *et al.*'s method and Ancuti *et al.*'s method. From left to right: (top) input haze imag, Kratz et al.'s result, Ancuti *et al.*'s result and our result. (bottom) the close-up patches in the box. (Best viewed in color)

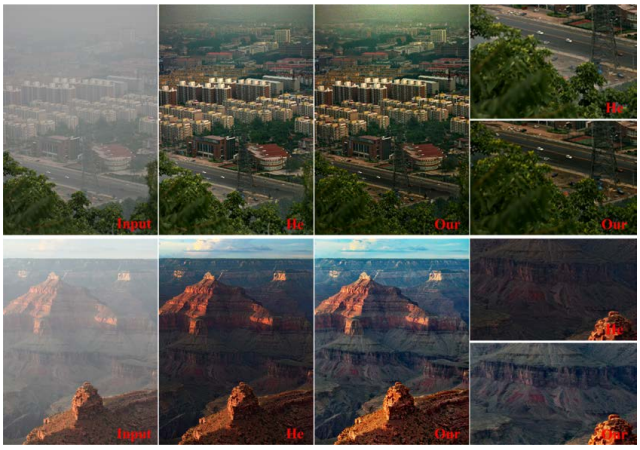

Figure 10. Comparisons with He *et al.*'s method. From left to right: input haze images, He *et al.*'s results, our results and the close-up patches. (Best viewed in color)

much from an exploration on the inherent boundary constraint on the transmission function. This constraint, together with a weighted L_1-norm based contextual regularization, is modeled into an optimization problem to recover the unknown transmission. An efficient algorithm using variable splitting is also proposed to solve the optimization problem. In comparison with the state-of-the-arts, our method can generate quite visually pleasing results with faithful color and finer image details and structures.

Single image dehazing often suffers from the problem of ambiguity between image color and depth. That is, a clean pixel may have the same color with a fog-contaminated pixel due to the effects of hazes. For example, some white objects in the scene often have a confusing color with the hazes. Therefore, without sufficient priors, these pixels are difficult to be reliably recognized as fog-contaminated or not fog-contaminated. This ambiguity, revealing the unconstraint nature of single image dehazing, often leads to excessive or inadequate enhancements on the scene objects.

From a geometric perspective of image dehazing, we have derived a boundary constraint on the transmission from the radiance cube of an image. Although the boundary constraint imposes a much weak constraint on the dehazing process, it proves to be surprisingly effective for the dehazing of most natural images, after combined with the contextual regularization. More generally, one can employ a tighter radiance envelop, not limited to a cubic shape, to provide a more accurate constraint on the transmissions. This may help to further reduce the ambiguity between color and depth, and avoid many erroneous enhancements on the image.

Another way to address the ambiguity problem is to adopt more sound constraints or develop new image priors, for example, using the scene geometry [2], or directly incorporating the available depth information [6] into the estimation of scene transmission. Although this may be unrealistic for generic image dehazing, it often works for particular applications, sine strict domain-related constraints may be easily derived in these applications.

Acknowledgment

The authors would like to thank the anonymous reviewers for their valuable remarks and suggestions. This work was supported in part by the National Basic Research Program of China (Grant No. 2012CB316304) and the Projects of the National Natural Science Foundation of China (Grant No. 61005036, 61175025, 61370039).

References

[1] C. O. Ancuti, C. Ancuti, C. Hermans, and P. Bekaert. A fast semi-inverse approach to detect and remove the haze from a single image. In *ACCV'11*, pages 501–514, 2011. 6

[2] P. Carr and R. Hartley. Improved single image dehazing using geometry. In *Digital Image Computing: Techniques and Applications*, pages 103–110, Dec. 2009. 8

[3] Z. Farbman, R. Fattal, D. Lischinski, and R. Szeliski. Edge-preserving decompositions for multi-scale tone and detail manipulation. In *ACM SIGGRAPH 2008*, pages 67:1–67:10, 2008. 3

[4] R. Fattal. Single image dehazing. In *ACM SIGGRAPH 2008*, pages 72:1–72:9, 2008. 1, 2, 6

[5] K. He, J. Sun, and X. Tang. Single image haze removal using dark channel prior. In *CVPR'09*, pages 1956–1963, 2009. 1, 2, 3, 4

[6] J. Kopf, B. Neubert, B. Chen, M. Cohen, D. Cohen-Or, O. Deussen, M. Uyttendaele, and D. Lischinski. Deep photo: model-based photograph enhancement and viewing. In *ACM SIGGRAPH Asia 2008*, pages 116:1–116:10, 2008. 1, 8

[7] L. Kratz and K. Nishino. Factorizing scene albedo and depth from a single foggy image. In *ICCV'09*, pages 1701–1708, Oct. 2009. 1, 2, 6

[8] B. G. Kristofor, T. V. Dung, and Q. N. Truong. An investigation of dehazing effects on image and video coding. *IEEE TIP*, 21(2):662–673, 2012. 1

[9] S. G. Narasimhan and S. K. Nayar. Vision and the atmosphere. *IJCV*, 48(3):233–254, 2002. 1

[10] S. G. Narasimhan and S. K. Nayar. Contrast restoration of weather degraded images. *IEEE TPAMI*, 25(6):713–724, 2003. 1, 2

[11] Y. Y. Schechner, S. G. Narasimhan, and S. K. Nayar. Instant dehazing of images using polarization. In *CVPR'01*, volume 1, pages 325–332, 2001. 1

[12] S. Shwartz, E. Namer, and Y. Y. Schechner. Blind haze separation. In *CVPR'06*, volume 2, pages 1984–1991, 2006. 1

[13] R. T. Tan. Visibility in bad weather from a single image. In *CVPR'08*, pages 1–8, 2008. 1, 2, 6

[14] J. P. Tarel and N. Hautiere. Fast visibility restoration from a single color or gray level image. In *ICCV'09*, pages 2201–2208, Oct. 2009. 1, 6

[15] J. P. Tarel, N. Hautiere, A. Cord, D. Gruyer, and H. Halmaoui. Improved visibility of road scene images under heterogeneous fog. In *IV'10*, June 2010. 6